Soft Matter

Dynamic Article Links

Cite this: *Soft Matter*, 2011, **7**, 1868

www.rsc.org/softmatter

PAPER

Gradient composition distribution in poly(2,6-dimethylphenylene oxide)/polystyrene blend nanorods†

Hui Wu,[a] Zhaohui Su[b] and Atsushi Takahara*[a]

Received 12th September 2010, Accepted 24th November 2010
DOI: 10.1039/c0sm00968g

We report formation of nanorods that exhibit a gradient distribution of poly(2,6-dimethylphenylene oxide) and polystyrene (PPO and PS), *i.e.*, the PPO weight fractions in the nanorods increase from top to bottom along the long axis of the nanorods. PPO/PS nanorods with various diameters were prepared by infiltrating porous anodic aluminium oxide (AAO) templates with polymer blend melts. Their morphology was investigated by Fourier transform infrared spectroscopy (FTIR). The gradient distribution of polymer blends in the nanopores is governed by (1) the viscosity difference between the two polymers and (2) the pore diameter. This remains true although PPO/PS blends are compatible in the segmental level. For various diameter nanorods made of PPO/PS blends, the PPO content decreased as the rod diameter became smaller owing to the increased confinement imposed by the nanopores. This leads to a higher rate of capillary rise in smaller nanopores.

Introduction

Polymer nanomaterials are of scientific and technological interest due to their unique properties and intriguing applications in many areas, such as microelectronics, optical, mechanical, and biomedical devices.[1,2] Various methods have been utilized to generate well-defined one dimensional (1D) nanostructures, such as self-assembly of microphase-separated block copolymers,[3–5] electrospinning,[6–8] nanoimprint lithography (NIL),[9–11] and template wetting.[12–27] Among the developed preparation methods, use of porous anodic aluminium oxide (AAO) templates for fabrication of polymeric nanostructures has drawn significant attention.[12–27] Unlike other methods for generating 1D nanostructures, formation of polymer nanotubes or nanorods *via* template wetting is based on the fact that polymer melts or polymer solutions with low surface-energy tend to wet the nanopore walls of templates with high surface-energy. Generally, AAO membranes possessing aligned, rigid, and separated cylindrical nanopores are ideal templates for the preparation of polymer nanomaterials with monodisperse diameters ranging from the nanoscale to the microscale. The thermal stability and mechanical rigidity of the inorganic alumina wall provide a strictly constrained environment and avoid breakdown of the cylindrical confinement. *Via* a two-step anodization process, self-ordered porous AAO is obtainable with pore sizes ranging from about 15 nm up to a few hundred nm and pore depths from several nm to several hundred μm. Pore diameter and monodispersity can be controlled by adjusting the anodization conditions (type of electrolyte, applied voltage, and pore-widening time), and pore depths can be controlled by the anodization time. Feature size and shape of the fabricated nanomaterials are easily controlled by distribution of the template pores. Thus, this highly versatile approach allows fabrication of polymeric nanomaterials with high aspect ratios (length/diameter), such as polymer nanotubes or nanorods, with novel morphology,[12–15] specific crystal orientation,[16–22] segmental dynamic behavior,[21–23] and polymorphic behavior.[25] Due to interactions between polymer blocks and pore walls, commensurability between pore diameter and the natural period of block copolymers (BCPs) morphology in the bulk, and the curvature that is forced on the BCPs morphology, phase-separating BCPs in AAO nanopores can break the bulk balance and self-assemble into a variety of structures, such as concentric lamellae, core shell cylinders, stacked disks, torus-like morphologies, and helical morphologies.[12–15] For semi-crystalline nanorods, the *c*-axes of polymer crystals developed in cylindrical nanopores preferentially oriented perpendicular to the long axis of the nanopore.[16–22] The crystallinity[17–20] and melting temperature[18,22] were reduced in contrast to the bulk owing to the spatial confinement of nanopores. Furthermore, an interesting crystal phase transition occurred, that is, the α-nonpolar crystal formed in poly(vinylidene fluoride) (PVDF) bulk film transformed into a ferroelectric γ-type crystal in alumina nanopores.[20]

Blending is a flexible way of producing new materials based on readily available polymers, and it has been demonstrated that polymer blends can exhibit a combination of properties

[a]*Institute for Materials Chemistry and Engineering, Kyushu University, Fukuoka, 819-0395, Japan. E-mail: takahara@cstf.kyushu-u.ac.jp*
[b]*State Key Laboratory of Polymer Physics and Chemistry, Changchun Institute of Applied Chemistry, Chinese Academy of Sciences, Changchun, Jilin, 130022, PR China*

† Electronic supplementary information (ESI) available: Determination of PPO content in PPO/PS blends by FTIR. See DOI: 10.1039/c0sm00968g

unattainable in any single polymer component.[28] For instance, poly(2,6-dimethylphenylene oxide)/polystyrene (PPO/PS) is a commercially successful polymer blend with good dimensional stability, high resistance to moisture, impact resistance, low temperature impact strength, low creep, and good processability. It is widely used in automotive instrument panels, interior trim, business equipment chassis, electrical applications, and medical equipment. It is conceivable that polymer blends can lead to nanomaterials and nanodevices with unique properties. Even though many reports are available in the literature on effects of nanoconfinement on BCPs[12–15] and homopolymers,[16–21,23–26] only few studies[27] based on polymer blends in nanopores have been reported. Also, from the view point of confinement effect, the PPO/PS system is interesting. The authors reported ultra-thinning-induced phase separation of polystyrene/poly(vinyl methyl ether) (PS/PVME) blend ultrathin films and that wetting of one component induced phase separation of PVME.[29] Similar behavior can be expected for blend nanorods. However, it has not systematically studied how the nanoconfinement changes the state of phase separation of miscible polymer blends in AAO templates. Here, we demonstrate polymer blend nanorods with gradient composition distribution can be prepared by melt-wetting PPO/PS blends through porous AAO templates.

Experimental

Sample preparation

The polymers used were PPO (M_n = 15 500, M_w/M_n = 2.16, Aldrich) and atactic PS (M_n = 115 000, M_w/M_n = 1.04, Polymer Source, Inc.). A PPO/PS blend with a composition of 50 : 50 (w/w) was prepared by casting from $CHCl_3$ solution. After the solvent had evaporated, the film was compression molded at 280 °C into a PPO/PS blend film with a thickness of 200 μm. AAO templates with pore diameters of 300, 65 and 35 nm and pore depths of ~140 μm were prepared *via* a two-step anodization as described elsewhere.[30,31] A porous AAO template was placed on top of the compression-molded PPO/PS blend film, and PPO/PS blend nanorods were obtained by annealing the film/AAO assembly at 280 °C for 8 h under vacuum. To prepare the PPO/PS nanorods for SEM and FTIR measurement, the template/blends assembly was immersed in 5 wt% phosphoric acid solution for 36 h to remove the inorganic AAO templates, leaving an array of PPO/PS nanorods protruding from the PPO/PS film. Thin slices of the cross-section of PPO/PS film with protruding nanorods for SEM observation and micro-FTIR analysis were cut using a razor blade after removal of the AAO template using phosphoric acid solution. The process for preparation of the polymer blend nanorods is schematically presented in Fig. 1.

Characterization

The morphology of AAO templates and the PPO/PS nanorods was investigated using S-4300SE (Hitachi Co., Ltd.) scanning electron microscope at an accelerating voltage of 5 kV. The PPO/PS composition in the polymer blend nanorods/film was analyzed by micro-Fourier transform infrared spectroscopy (micro-FTIR) on a PerkinElmer Spectrum One spectrometer in connection with an Autoimage microscope equipped with a MCT detector operating in the transmission mode. The microscope includes a viewing system that magnifies the optical image of the sample so that a point of interest in the sample can be found, seen, and analyzed. FTIR spectra were collected at 2 cm^{-1} resolution with 128 scans coadded. The aperture size was 300 × 25 μm^2 and the resolution along the long axis of the rod was 25 μm. At least three replicate samples were prepared for FTIR analyses.

Results and discussion

The polymer blend nanorods were prepared by melt wetting. Inorganic materials like AAO templates are considered high surface energy materials, whereas most polymers (*e.g.* PPO and PS) are of lower surface energies. Thus, the low-energy polymer melts can wet the high-energy surfaces easily. The wetting of the pore walls by the polymer melts causes a capillary rise of the polymer melts into the nanopores, leading to polymer nanorod formation.[17] Fig. 2d–f show the SEM images of PPO/PS blend nanorods with diameters of 300, 65, and 35 nm respectively that were prepared by infiltrating AAO templates (Fig. 2a–c) with PPO/PS blend melts. Transmission electron microscopy (TEM) observation also confirmed that the generated nanomaterials were solid rods, not hollow tube structures (data not shown).

Micro-FTIR provides a simple and powerful approach for local analysis that is rapid and nondestructive. Micro-FTIR measurements of blend composition were performed at different

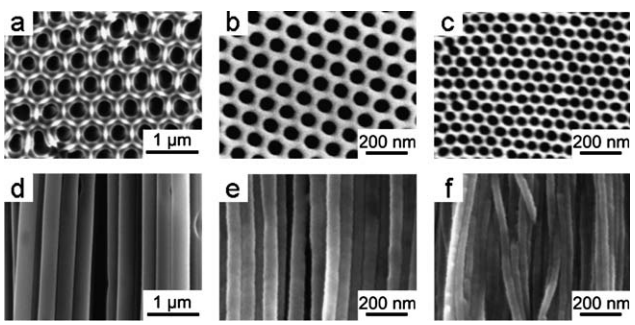

Fig. 2 SEM micrographs of AAO templates with diameters of: (a) 300 nm, (b) 65 nm, (c) 35 nm, and PPO/PS nanorods with diameters of: (d) 300 nm, (e) 65 nm, and (f) 35 nm.

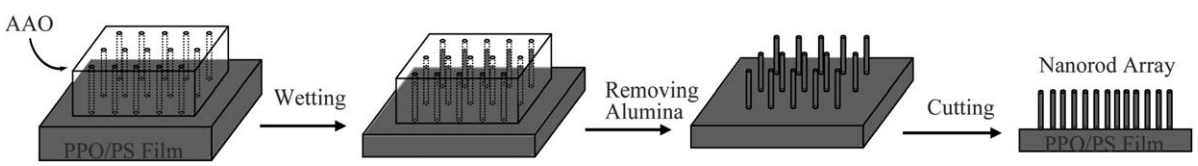

Fig. 1 Schematic procedure for the preparation of PPO/PS nanorods.

positions of the nanorods/film. Fig. 3A shows the optical micrograph of a thin slice of the PPO/PS nanorods/film prepared with an AAO template comprised of 300 nm diameter pores. The area on the top of the micrograph is the nanorod array protruding from the bulk film after removal of the AAO template, which appears darker due to the scattering of light at the numerous nanorod/air interfaces, while the translucent section on the bottom of the micrograph is the cross-section of the residual PPO/PS film.[17] The length of the nanorods of 300 nm diameter is about 78 μm, and the nanorod array is supported by the bulk film to prevent nanorod disarray. During the measurement, the scan area was 300 × 25 μm^2 and the resolution along the long axis of the rod was 25 μm. This was to ensure that spectra from the top to the bottom of the sample were obtained. Fig. 3B presents the corresponding micro-FTIR spectra at different measured positions in Fig. 3A. The top three spectra are of nanorods at the positions *a*, *b*, and *c*, while the bottom three spectra represent the residual bulk film at positions *d*, *e*, and *f*, respectively. It is known that the peak at 959 cm^{-1} in the spectrum of the blend is due to in-plane CH wagging of the tetra-substituted phenylene ring of PPO[32] and the band at 906 cm^{-1} is out-of-plane CH wagging of the benzene ring of PS.[33] Sample information, such as the weight fraction of each component, can be obtained by examining these two specified bands in FTIR spectra. To make a qualitative analysis among different positions in the sample, for all the datasets, the intensities (peak height) of the bands were normalized to that of the 906 cm^{-1} band. When this was done, the intensity of the 959 cm^{-1} band in all the spectra of the nanorods increased from position *a* to position *c*, indicating the PPO weight fraction in the nanorods increased from the top side to the bottom side. These results show a gradient composition distribution formed in the PPO/PS nanorods along the long axis of nanorods.

In order to understand the effect of geometric confinement of nanopores on the morphology of polymer blends, PPO/PS nanorods with smaller diameters were investigated. Because the intensities of the bands in all spectra were normalized to that of the 906 cm^{-1} band, we could make comparisons among different spectra to get information of the relative PPO content at different positions. For nanorods made of PPO/PS blends within nanopores of 65 (Fig. 4) and 35 nm diameter (Fig. 5), the intensity of the 959 cm^{-1} band increased from the top to the bottom of the nanorods. This indicates that a gradient composition distribution was formed in nanorods for pores of these sizes as well. More strikingly, when the spectra of the 65 nm and 300 nm diameter nanorods were compared, the signal was weaker at position *a* in the spectrum of the 65 nm nanorods than in the spectrum of the 300 nm nanorods. Similarly, a reduction in intensity at positions *b* and *c* was observed in the 65 nm nanorod spectra compared to the 300 nm nanorod spectra. This suggests the overall PPO content in the 65 nm diameter nanorods was less than that in nanorods of 300 nm diameter. Finally, when comparing the spectra of the 35 nm diameter nanorods to the 65 nm diameter nanorods similar trends were seen at positions *a*, *b*, and *c*; that is a decrease of intensity was seen in the spectra of the smaller diameter nanorods. Altogether these data revealed a trend, PPO content decreased as the degree of confinement increased. Indeed, the molecular compositional distribution of polymer blends in nanopores is strongly influenced by the degree of confinement imposed by the nanopores.

On the basis of various known compositions of the PPO/PS blends, the following equations can be obtained to extract the absolute PPO content in a particular PPO/PS blend from its IR spectrum (see ESI†):

$$C_{\mathrm{PPO}} = \frac{A_{959}}{A_{959} + 3.69A_{906}} \quad (1)$$

$$C_{\mathrm{PS}} = 100\% - C_{\mathrm{PPO}} \quad (2)$$

where C_{PPO} and C_{PS} represent the content of PPO and PS in the PPO/PS blends, A_{959} and A_{906} are the respective band area for the peaks at 959 and 906 cm^{-1}, 3.69 is the ratio of absorptive coefficients of 959 cm^{-1} band to 906 cm^{-1} band.

Table 1 lists the PPO content for both nanorods and the bulk at different positions extracted from the FTIR data according to eqn (1). The PPO contents in the nanorods of 300 nm diameter at positions *a*, *b*, and *c* are 37.5%, 45.4%, and 53.1%, respectively,

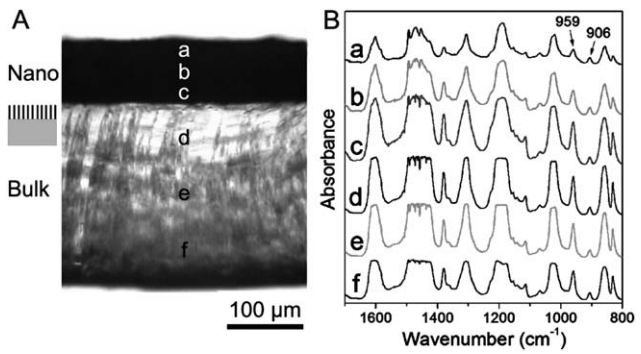

Fig. 3 (A) Optical micrograph of a thin slice of a PPO/PS nanorods/film prepared with an AAO template comprised of 300 nm diameter pores. The darker section on the top is the nanorod array. To the left is a schematic of nanorods connected with bulk film. (B) Corresponding micro-FTIR spectra at the measured positions. The spatial resolution at each position is 300 × 25 μm^2 and the peak intensities are normalized to 906 cm^{-1} band.

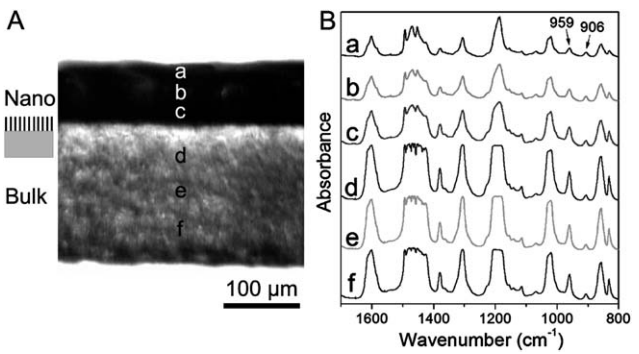

Fig. 4 (A) Optical micrograph of a thin slice of a PPO/PS nanorods/film prepared with an AAO template comprised of 65 nm diameter pores. The darker section on the top is the nanorod array. To the left is a schematic of nanorods connected with bulk film. (B) Corresponding micro-FTIR spectra at the measured positions. The spatial resolution at each position is 300 × 25 μm^2 and the peak intensities are normalized to 906 cm^{-1} band.

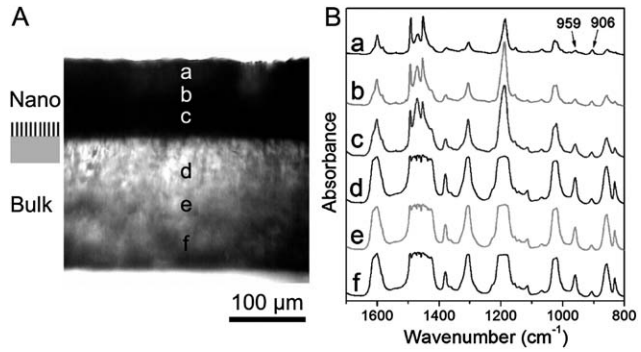

Fig. 5 (A) Optical micrograph of a thin slice of a PPO/PS nanorods/film prepared with an AAO template comprised of 35 nm diameter pores. The darker section on the top is the nanorod array. To the left is a schematic of nanorods connected with bulk film. (B) Corresponding micro-FTIR spectra at the measured positions. The spatial resolution at each position is 300 × 25 μm^2 and the peak intensities are normalized to 906 cm^{-1} band.

Table 1 Comparison of PPO content at different positions in PPO/PS blend nanorods/film

	Nanorods (%)			Bulk (%)		
Rod diameters	*a*	*b*	*c*	*d*	*e*	*f*
300 nm	37.5	45.4	53.1	53.2	52.5	50.7
65 nm	27.9	33.0	42.2	54.9	51.9	50.6
35 nm	13.8	25.1	40.8	54.5	52.6	50.6

clearly showing the PPO content in nanorods increased from the top (position *a*) to the bottom (position *c*) of the nanorods and a gradient composition distribution was formed in the nanorods. These trends were also observed in the nanorods of 65 and 35 nm diameters from the detailed values in Table 1. The content of PPO in nanorods of 35 nm diameter was much lower than that in the 65 and 300 nm diameters, indicating the PPO component with higher viscosity is more difficult to enter into the smaller nanopores due to the stronger spatial confinement of nanopores. Although PPO/PS blends are compatible on the segmental level due to the strong van der Waals interaction between the phenyl ring of PS and the phenylene ring of PPO,[34] the polymer blend melts are forced to separate to form gradient composition distribution nanorods during the capillary flow.

From Table 1, it is worth noting that the average PPO content in nanorods was less than that in bulk. The lower PPO content reflects the higher PS content in the nanorods as compared with the bulk, indicating the PS components preferentially enter into the nanopores during the capillary flow. For the polymers of PPO/PS, it is well known that the melt viscosity of PPO is much higher than PS and the addition of PS can improve the processability of PPO.[28] The larger the melt viscosity is, the more slowly it flows. Under the same condition, the component with lower melt viscosity has higher mobility to enter nanopores *via* the capillary force. Therefore, the PS component entered into the nanopores more easily than the PPO component and caused a higher content of PS in the nanopores. Meanwhile, under the capillary force, the PS component tries to slip the *leash* of the PPO component (the strong interaction between the phenyl ring of PS and the phenylene ring of PPO) and leaves large amounts of the PPO component at the position *d*, causing the PPO content at position *d* to be a little higher than at position *e* and *f*. For the blend melt within the nanopores, the PS component keeps moving upward to shake off the *bondage* of the PPO component, and leaves PPO component behind, leading to higher weight fraction of PS in the top of nanorods than that in the bottom. Consequently, a gradient distribution of polymer composition is formed in the nanorods along the long axis of rods. As the wetting time increases, the gradient of polymer components in nanopores develops, causing more significant composition difference between the top side and the bottom side of the nanorods.

It is reported that polystyrene of low molecular weights wetted alumina nanopores with much higher rates than that of high molecular weights.[24] This result showed that the polystyrene with low viscosity is enriched in nanopores, which is consistent with our results. For the polymers we used, owing to the polydispersity (2.16) of the PPO component, it is reasonable to deduce that the content of low molecular weight PPO in nanopores is higher than that in the bulk and a gradient distribution of different molecular weight PPO is also formed in the blend nanorods.

We now turn our attention to the effects of nanorod length in various nanopores on the ability of the polymer blend melts to fill up the void space of nanopores. The surface tension, viscosity of the polymer melt and the size of the nanopore determine the rate of flow so that the length of nanorods is given by[9,13]

$$z = \left(\frac{Rt\gamma\cos\theta}{2\eta}\right)^{1/2} \quad (3)$$

where z is the length of the column of polymer melts in the nanopore, R is the hydraulic radius (the cross-sectional area of a stream divided by the wetted perimeter; R is one half the radius of nanopore), t is the time, γ is the surface tension of the polymer melts, θ is the contact angle at the polymer/capillary wall interface, and η is the viscosity of the polymer melt.

Because the polymer blends in nanopores have a gradient composition distribution, some parameters on the right side of eqn (3) (γ, θ, and η) become undetermined. Therefore it is difficult to predict a precise length of the column of polymer melts in nanopores. However, we can make a comparison of the relative length of polymer blend melts within various nanopores after the capillary flow between the prediction and the experiments. If the blends entering into the various nanopores have the same composition, the rate of capillary rise is only dependent on the pore size of the AAO templates. Therefore, the ratio of capillary rise in the nanopores of 300, 65, and 35 nm should have the relationship of $z_{300} : z_{65} : z_{35} = R_{300}^{1/2} : R_{65}^{1/2} : R_{35}^{1/2} = 1 : 0.47 : 0.34$. That is when pore diameters become smaller, the rate of capillary rise reduces as the polymer melts fill up the void space by capillary force. Fig. 6A shows the predicted relative lengths of polymer blend melts within nanopores of 300, 65, and 35 nm.

From the optical images of PPO/PS nanorods (Fig. 3A, 4A and 5A), under the same annealing conditions (280 °C for 8 h), the average length of nanorods (capillary rise) of 300, 65, and 35 nm diameter is about 78, 76, and 96 μm (each number is an average of 3 replicates), respectively. For comparison, the lengths

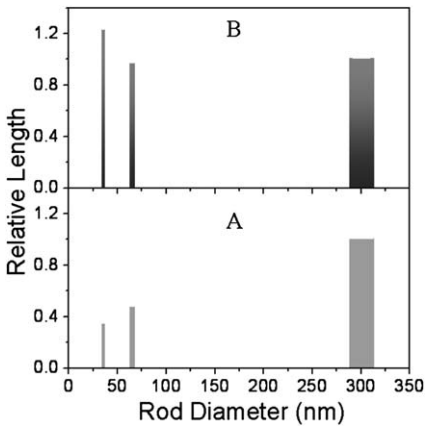

Fig. 6 Comparison of predicted data (A) with experimental data (B) of the relative length of polymer blend melts within nanopores of 300, 65, and 35 nm after the capillary flow.

of nanorods with various diameters are normalized to those of the 300 nm diameter nanorods. Then, the relative length of the 300, 65, and 35 nm diameter nanorods is 1, 0.97, and 1.23, respectively (Fig. 6B). With the 300 nm diameter nanorods as a reference, the relative length of the 65 nm diameter nanorods (0.97) is larger than its predicted value (0.47), revealing the rate of capillary rise in 65 nm diameter nanopores is higher than that in nanopores of 300 nm diameter. For the polymer blends in the smaller nanopores of 35 nm diameter, the relative length (1.23) is much longer than the predicted (0.34), showing the trend that the rate of capillary rise in nanopores increases as the degree of confinement increases. The increased rate of capillary rise indicates a higher mobility of polymer blend melt in smaller nanopores, corroborating that the viscosity of polymer blend melts in smaller nanopores is lower than that in larger ones, which is caused by the higher PS content of polymer blends in smaller nanopores. Apparently, the length measurement results are in good agreement with the FTIR results. During the capillary flow of polymer blends in various nanopores, the PPO component with a higher viscosity, has a more difficult time entering into smaller nanopores due to the stronger confinement of nanopores, the resulting PPO content in smaller nanopores is less than that in larger ones. Therefore, as the degree of confinement increases, the PS content with lower viscosity in blend nanorods increases, leading a to higher rate of capillary rise in smaller nanopores.

Conclusions

PPO/PS blend nanorods were prepared by infiltrating porous AAO templates with polymer blend melts and the morphology of PPO/PS blends in various diameter nanopores were investigated by FTIR. Gradient composition distribution of polymer blend nanorods was formed in nanopores, though PPO/PS blends are compatible on the segmental level. The molecular aggregation states of polymer blends in nanopores are governed by the viscosity difference of the polymers and degree of confinement of pore diameter during the capillary flow into nanopores. The component with higher viscosity had lower mobility to enter into nanopores, causing the PPO weight fraction in nanorods to decrease from bottom to top along the long axis of the nanorod. For the PPO/PS blends in various diameter nanorods, the PPO content decreased as the rod diameter became smaller owing to the stronger confinement of nanopores, causing a higher rate of capillary rise in smaller nanopores. The capillary wetting of porous AAO templates by polymer blends offers a unique method for preparation of functional nanostructured materials with gradient composition distribution. This allows us to envisage that the gradient nanomaterials may have properties such as gradient refractive index, improved strength against thermal stress and gradient mechanical modulus for the potential application to optical nanodevices, and that the nanorod array with stable mechanical properties also has a possibility to be applied to gecko-tape and biofluidic devices.

Acknowledgements

The present work was supported by a Grant-in-Aid for the Global COE Program "Science for Future Molecular Systems" from the MEXT, Japan. Z.S. thanks the National Natural Science Foundation of China (20774097, 50921062) for support.

References

1 C. R. Martin, *Science*, 1994, **266**, 1961.
2 M. Steinhart, *Adv. Polym. Sci.*, 2008, **220**, 123.
3 P. Huang, L. Zhu, S. Z. D. Cheng, Q. Ge, R. P. Quirk, E. L. Thomas, B. Lotz, B. S. Hsiao, L. Z. Liu and F. J. Yeh, *Macromolecules*, 2001, **34**, 6649.
4 S. Nojima, Y. Ohguma, K. Kadena, T. Ishizone, Y. Iwasaki and K. Yamaguchi, *Macromolecules*, 2010, **43**, 3916.
5 T.-M. Chung, T.-C. Wang, R.-M. Ho, Y.-S. Sun and B.-T. Ko, *Macromolecules*, 2010, **43**, 6237.
6 D. Li and Y. N. Xia, *Adv. Mater.*, 2004, **16**, 1151.
7 Y. Liu, L. Cui, F. X. Guan, Y. Gao, N. E. Hedin, L. Zhu and H. Fong, *Macromolecules*, 2007, **40**, 6283.
8 L. A. Smith, X. H. Liu and P. X. Ma, *Soft Matter*, 2008, **4**, 2144.
9 K. Y. Suh, Y. S. Kim and H. H. Lee, *Adv. Mater.*, 2001, **13**, 1386.
10 Z. J. Hu and A. M. Jonas, *Soft Matter*, 2010, **6**, 21.
11 K. Honda, M. Morita, H. Masunaga, S. Sasaki, M. Takata and A. Takahara, *Soft Matter*, 2010, **6**, 870.
12 K. Shin, H. Q. Xiang, S. I. Moon, T. Kim, T. J. McCarthy and T. P. Russell, *Science*, 2004, **306**, 76.
13 H. Q. Xiang, K. Shin, T. Kim, S. I. Moon, T. J. McCarthy and T. P. Russell, *Macromolecules*, 2004, **37**, 5660.
14 Y. M. Sun, M. Steinhart, D. Zschech, R. Adhikari, G. H. Michler and U. Gösele, *Macromol. Rapid Commun.*, 2005, **26**, 369.
15 P. Dobriyal, H. Xiang, M. Kazuyuki, J.-T. Chen, H. Jinnai and T. P. Russell, *Macromolecules*, 2009, **42**, 9082.
16 M. Steinhart, P. Göring, H. Dernaika, M. Prabhukaran, U. Gösele, E. Hempel and T. Thurn-Albrecht, *Phys. Rev. Lett.*, 2006, **97**, 027801.
17 H. Wu, W. Wang, H. Yang and Z. Su, *Macromolecules*, 2007, **40**, 4244.
18 K. Shin, E. Woo, Y. G. Jeong, C. Kim, J. Huh and K. W. Kim, *Macromolecules*, 2007, **40**, 6617.
19 H. Wu, W. Wang, Y. Huang and Z. Su, *Macromol. Rapid Commun.*, 2009, **30**, 194.
20 M. C. Garcia-Gutierrez, A. Linares, J. J. Hernandez, D. R. Rueda, T. A. Ezquerra, P. Poza and R. J. Davies, *Nano Lett.*, 2010, **10**, 1472.
21 J. Martin, C. Mijangos, A. Sanz, T. A. Ezquerra and A. Nogales, *Macromolecules*, 2009, **42**, 5395.
22 J. L. Lutkenhaus, K. McEnnis, A. Serghei and T. P. Russell, *Macromolecules*, 2010, **43**, 3844.
23 A. Serghei, D. Chen, D. H. Lee and T. P. Russell, *Soft Matter*, 2010, **6**, 1111.
24 M. F. Zhang, P. Dobriyal, J. T. Chen, T. P. Russell, J. Olmo and A. Merry, *Nano Lett.*, 2006, **6**, 1075.
25 H. Wu, W. Wang, Y. Huang, C. Wang and Z. Su, *Macromolecules*, 2008, **41**, 7755.

26 K. Shin, S. Obukhov, J. T. Chen, J. Huh, Y. Hwang, S. Mok, P. Dobriyal, P. Thiyagarajan and T. P. Russell, *Nat. Mater.*, 2007, **6**, 961.
27 D. Chen, J. T. Chen, E. Glogowski, T. Emrick and T. P. Russell, *Macromol. Rapid Commun.*, 2009, **30**, 377.
28 L. A. Utracki, *Polymer Alloys and Blends*, Hanser Publ., New York, 1989.
29 K. Tanaka, J. S. Yoon, A. Takahara and T. Kajiyama, *Macromolecules*, 1995, **28**, 934.
30 H. Masuda and K. Fukuda, *Science*, 1995, **268**, 1466.
31 A. P. Li, F. Muller, A. Birner, K. Nielsch and U. Gösele, *J. Appl. Phys.*, 1998, **84**, 6023.
32 K. Nakashima, Y. Ren, T. Nishioka, N. Tsubahara, I. Noda and Y. Ozaki, *J. Phys. Chem. B*, 1999, **103**, 6704.
33 C. Y. Liang and S. Krimm, *J. Polym. Sci.*, 1958, **27**, 241.
34 S. T. Wellinghoff, J. L. Koenig and E. Baer, *J. Polym. Sci., Part B: Polym. Phys.*, 1977, **15**, 1913.